Scanning Laser-Beam-Induced Current Measurements of Lateral Transport Near-Junction Defects in Silicon Heterojunction Solar Cells

Michael G. Deceglie, Hal S. Emmer, Zachary C. Holman, Antoine Descoeudres, Stefaan De Wolf, Christophe Ballif, and Harry A. Atwater

***Abstract*—We report the results of scanning laser-beam-induced current (LBIC) measurements on silicon heterojunction solar cells that indicate the length scale over which photogenerated carriers are sensitive to local defects at the amorphous silicon/crystalline silicon heterojunction interface. The defects were intentionally created with focused ion beam irradiation, enabling us to study how defects at a predefined and known location affect carrier collection and transport in neighboring regions where the device remains pristine. The characteristic length scale over which carriers in the pristine areas of the device are vulnerable to loss via recombination in the adjacent defective region increases to over 50 μm as the device is forward biased. For photocarriers generated near the amorphous–crystalline interface, LBIC measurements suggest that lateral transport in the near-junction inversion layer in the c-Si is an important transport mechanism.**

***Index Terms*—Carrier transport, device physics, heterojunction with intrinsic thin layer (HIT), laser-beam-induced current (LBIC), silicon heterojunction (SHJ).**

I. Introduction

Silicon heterojunction (SHJ) solar cells, based on a heterojunction between hydrogenated amorphous silicon (a-Si:H) and a crystalline silicon (c-Si) absorber, are a promising approach to high-efficiency silicon-based photovoltaics. They are notable for their high open-circuit voltage ($V_{\rm oc}$), which can exceed 720 mV [1], [2]. In their most common implementation, SHJ cells employ a thin region of intrinsic a-Si:H to passivate the c-Si surface; this approach was pioneered by Sanyo with the heterojunction with intrinsic thin layer (HIT) cell [3], [4]. The deposition of a-Si:H at low temperature, which is usually via plasma-enhanced chemical vapor deposition (PECVD), benefits cell manufacturing by eliminating high-temperature diffusion steps. SHJ devices are also known to maintain their performance better than homojunction devices at elevated operating temperature; this characteristic is associated with the high $V_{\rm oc}$ in SHJ cells [4]–[6]. This is an important consideration for photovoltaic system performance in realistic operating conditions. In addition, this approach is considered to be an enabling technology for thin c-Si absorber designs [7]. The $V_{\rm oc}$ of SHJ cells is known to be sensitive to the quality of the interface between the a-Si:H and the c-Si [5], [8]–[12].

SHJs have been observed by others to exhibit a conductive inversion layer in the c-Si region just below the heterojunction [13]–[18]. The inversion layer, which is a result of the band offsets and quasi-Fermi levels, is shown in Fig. 1; inversion

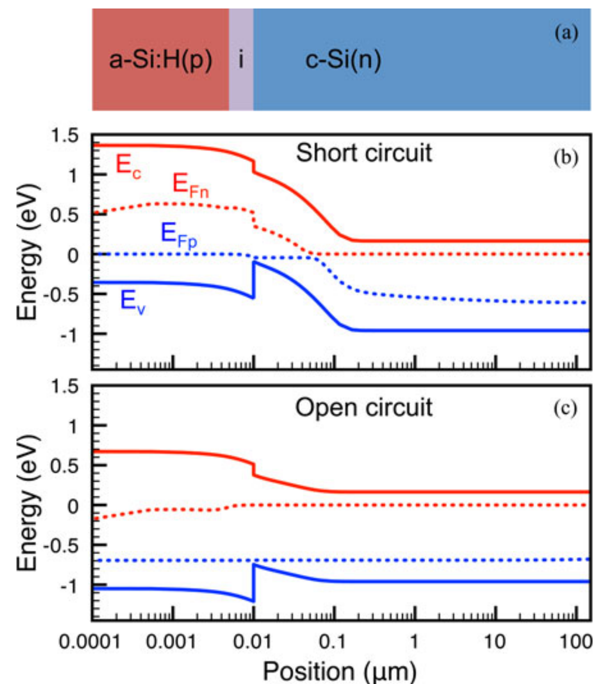

Fig. 1. (a) Schematic of an SHJ; layers are aligned with the position axis of (b) and (c). (b) Simulated band diagram for an SHJ at short circuit under AM1.5G illumination. (c) Simulated band diagram for an SHJ at open circuit under AM1.5G illumination. The inversion layer is apparent in (b) and (c), where the hole quasi-Fermi level is close to the valence band edge on the c-Si side of the heterojunction. E_c is the conduction band, E_v is the valance band, E_{Fp} is the hole quasi-Fermi level, and E_{Fn} is the electron quasi-Fermi level.

Manuscript received February 28, 2013; revised October 10, 2013; accepted October 21, 2013. Date of publication November 20, 2013; date of current version December 16, 2013. The work of M. G. Deceglie, H. S. Emmer, and H. A. Atwater was supported by the National Science Foundation (NSF) and the Department of Energy under Grant NSF CA No. EEC-1041895, the Caltech Taiwan Energy Exchange, and the Bay Area Photovoltaics Consortium. The work of Z. C. Holman, A. Descoeudres, S. De Wolf, and C. Ballif was supported by the European Union Seventh Framework Programme, Axpo Naturstrom Fonds, and the Swiss Commission for Technology and Innovation.

M. G. Deceglie, H. S. Emmer, and H. A. Atwater are with the Thomas J. Watson Laboratories of Applied Physics and the Kavli Nanoscience Institute, California Institute of Technology, Pasadena, CA 91125 USA (e-mail: michael.deceglie@gmail.com; hemmer@caltech.edu; haa@caltech.edu).

Z. C. Holman, A. Descoeudres, S. De Wolf, and C. Ballif are with the École Polytechnique Fédérale de Lausanne, Institute of Microengineering, Photovoltaics and Thin-Film Electronics Laboratory, Neuchâtel 2000, Switzerland (e-mail: zachary.holman@asu.edu; antoine.descoeudres@epfl.ch; stefaan.dewolf@epfl.ch; christophe.ballif@epfl.ch).

Color versions of one or more of the figures in this paper are available online at http://ieeexplore.ieee.org.

Digital Object Identifier 10.1109/JPHOTOV.2013.2289353

2156-3381 © 2013 IEEE

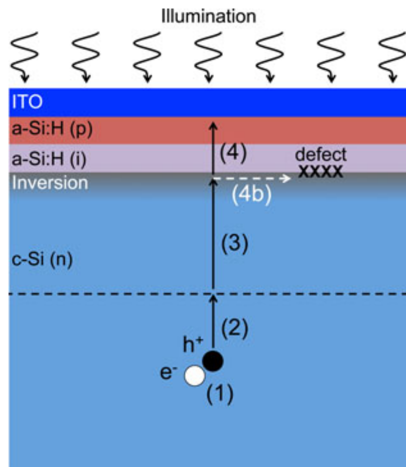

Fig. 2. Schematic illustration of carrier collection in SHJ solar cells at biases significantly below V_{oc}. (1) Electron–hole pairs are photogenerated in the base. (2) Minority carriers diffuse to the depletion region. (3) The built-in electrostatic field in the depletion regions sweeps carriers via drift into the inversion layer. (4) Carriers are collected from the inversion layer into the a-Si:H emitter. Carriers also move laterally in the inversion layer, increasing the probability that they encounter a local defect and recombine, as illustrated in (4b). The dashed black line indicates the depletion region edge.

occurs where the hole quasi-Fermi level comes close to the valence band edge on the c-Si side of the heterojunction. Here, we report the results of laser-beam-induced current (LBIC) measurements which probe lateral carrier flow in this inversion layer for device biases under 430 mV. Our results support the hypothesis that the collection of carriers photogenerated near the front of the device is hindered by lateral carrier transport in the inversion layer to defective regions of the junction. In addition, we find that the length scale over which carriers are sensitive to nearby defects increases in forward bias. Thus, this study elucidates a physical mechanism that underlies the well-known sensitivity that SHJ cells show to interface quality.

The collection of photoexcited carriers in the base of an SHJ cell for device biases at which significant photocurrent is collected (near or below the maximum power point) can be intuitively understood as the series of processes illustrated in Fig. 2 for an n-type c-Si base. 1) Upon absorption of a photon, electron–hole pairs are excited in the c-Si(n) absorber. 2) The holes undergo minority carrier diffusion until they either recombine in the bulk or at the rear surface, or until they reach the depletion region. 3) The built-in electrostatic field in the depletion region sweeps the holes, via drift, into the inversion layer. 4) The holes are collected from the inversion layer through the a-Si:H(i) into the a-Si:H(p) emitter where they recombine with electrons at the contact, providing current to an external circuit. For photons absorbed within the depletion region, the process begins at step 2. In addition, carriers that are ultimately collected will, on average, only diffuse a lateral distance in the quasi-neutral region approximately equal to their distance from the depletion region edge. Note that the physical processes involved in step 4 are not yet fully understood [19]–[21].

We report the results of LBIC measurements designed to probe the dynamics of carrier transport that occur between steps 3 and 4 in SHJ solar cells. Our measurements support the hypothesis illustrated by pathway (4b) in Fig. 2 that carriers can flow laterally toward defects in the inversion layer at the a-Si:H/c-Si interface rather than being collected into the emitter (step 4) [22]. This process takes place with a characteristic surface sampling length that is found to increase under forward bias, indicating that carriers have an increased probability of encountering a localized recombination-active defect and, thus, being lost prior to collection under such conditions.

The experiment described here was designed to probe transport in the near-junction inversion layer. We accomplished this by generating photocurrent with laser wavelengths (633 and 488 nm) with relatively short absorption depths in c-Si, which resulted in photocarrier generation near the front junction. We note that these wavelengths are also (parasitically) absorbed in the TCO and a-Si:H layers but that a sufficient flux reaches the c-Si to produce measureable photocurrent [23]. Since carrier diffusion is isotropic in a homogeneously doped quasi-neutral absorber layer, it is expected that carriers can diffuse laterally in the quasi-neutral region over a distance roughly equivalent to their distance from the depletion edge. Thus, the carriers contributing to the LBIC signal would typically be expected to diffuse laterally a few microns (or less) in the quasi-neutral region prior to entering the depletion region. In addition, we conducted the experiment at voltages well below typical 1-sun open-circuit conditions ensuring that carriers reaching the front of the device are efficiently swept into the inversion layer by the internal field once they reach the depletion region edge. It is important to note that under 1-sun operating conditions, additional carriers would also be generated by longer wavelength light in the solar spectrum. Under these conditions, and especially near open circuit, lateral carrier diffusion in the quasi-neutral region (as opposed to mere inversion layer transport) also contributes substantially to transport and, thus, to the collection sensitivity to local defects.

II. Method

The LBIC experiment was carried out by scanning a focused laser beam over an SHJ device and using the resulting photocurrent as a function of laser position on the sample to form an image. The LBIC image thus indicates where useful photocurrent is generated in the device. In our implementation, we used a Zeiss Imager.Z2m microscope with an LSM 710 module and 0.25 NA objective to scan the laser beam over the sample. This produces a sub-5-μm-diameter laser spot. The resulting current signal was passed through a transimpedance amplifier with a gain of 10^5 Ω. The amplifier also enabled us to apply a dc bias to the device and, thus, collect bias-dependent photocurrent maps. We carried out the LBIC experiment with laser wavelengths of both 633 and 488 nm under dark background conditions (i.e., no bias illumination was used). Note that because the device was placed in forward bias, the dark current flowing over the entire area of the sample (approximately 0.4 cm^2) created a dc offset to the current which competed with the LBIC signal, limiting the forward bias at which photocurrent could be extracted and an image could be formed. To obtain clear LBIC signals relative to the forward bias dark current dc offset, the laser power was

increased up to a factor of 2 for some measurements. We verified that this did not affect the shape of line profiles extracted from the LBIC images. For the purposes of this study, LBIC profiles were normalized such that they converge to a maximum value of unity far from any defective area.

To probe lateral transport, we performed the LBIC measurement on an SHJ cell with localized, intentionally induced defects at the heterojunction. The cells were fabricated using processes described in detail elsewhere [24]–[26]. Briefly, a-Si:H layers were deposited via PECVD onto polished n-type float-zone silicon wafers [(1 0 0) oriented, 280 μm thick, with a resistivity of 4 Ω·cm] after removing the native oxide in hydrofluoric acid. An intrinsic/p-type a-Si:H stack that was approximately 10 nm thick was deposited on the front side to collect holes, and an intrinsic/n-type a-Si:H stack that was approximately 15 nm thick was deposited on the rear side to collect electrons. To form the contacts, ITO was sputtered onto both sides of the wafers. In keeping with previous optimization [26], the target thickness and sheet resistance were 70 nm and 100 Ω/sq for the front ITO layer and 150 nm and 500 Ω/sq for the rear. A silver layer was then sputtered over the rear ITO layer, and a silver grid was screen printed on the front contact to finish the cells. The cells were 2×2 cm^2 in area.

The defects were created by irradiating a target area of the device with a 30-keV focused ion beam (FIB) of Ga ions. The irradiation was carried out for varying ion doses between 6×10^{12} and 6×10^{13} ions cm^{-2} over a 43 μm $\times$ 50 μm area of the cell, avoiding the contact grid. We note that in this application, the ion beam does not remove a significant amount of material as in typical applications of the FIB milling technique. Instead, we observed local performance degradation in SHJ devices after irradiation of the ITO top contact under typical FIB imaging conditions. Because FIB imaging conditions led to degradation and because imaging with the ion beam is necessary to properly focus it, we were unable to create point-like defects without degrading the surrounding area. Thus, we used the imaging area of a single frame as the defect to enable a controlled ion dose in a known location without adversely affecting the neighboring material. We attribute the observed reduction in photocurrent to damage to the junction caused by atoms scattered from the ITO layer. This is confirmed by Monte Carlo simulations [27] of Ga ions impinging on a 70-nm-thick ITO layer on Si, which indicated that while negligibly few Ga ions are expected to penetrate the full thickness of the ITO layer, forward scattered In, Sn, and O atoms reach the Si region. The advantage of inducing a defect of known size and location is that it can be used to probe the device physics in the pristine regions of the device immediately surrounding it. We also note that current flow from the TCO, through any shunts associated with the induced defect, contributes to the dark current dc offset (see above) and would not be expected to change the curvature of the LBIC signal in the defect region. This is because any current injected from the contact at forward bias would be present with or without the local laser illumination.

We also carried out finite-element simulations to elucidate some of the device physics associated with the experiment. The simulations were carried out with Synopsys TCAD with Sentaurus Device [28] using material parameters adapted from [29]. In these simulations, the c-Si base was 250 μm thick, doped n-type at 10^{15} cm^{-3}, and had a minority carrier lifetime of 1 ms. The doped and intrinsic a-Si:H layers were both 5 nm thick. We set the dielectric constant for a-Si:H to 11.9, the bandgap to 1.72 eV, the electron affinity to 3.94 eV, the effective density of states in both the conduction and valence band to 10^{20} cm^{-3}, the electron mobility to 20 cm^2·V^{-1}·s^{-1}, the hole mobility to 5 cm^2·V^{-1}·s^{-1}, and the thermal velocity for both electrons and holes to 4.27×10^4 cm·s^{-1}. The n-type a-Si:H back surface field had an active doping concentration of 3×10^{19} cm^{-3}, and the p-type a-Si:H emitter had an active doping concentration of 1×10^{19} cm^{-3}. Recombination in the a-Si:H was modeled with a continuum of trap states, with the distributions and capture cross sections taken from [29]. While these parameters reproduce experimental *I–V* curves, we only use the results of these simulations here for two auxiliary purposes: to calculate the SHJ band diagram (see Fig. 1) and to quantify the lateral diffusion of photoexcited carriers in the c-Si base that is not in the inversion layer. Because the exact microscopic mechanisms of charge carrier transfer across the interface are not yet fully understood, they cannot be exactly modeled [19]–[21]. Thus, we do not claim to have developed a physically relevant and comprehensive model of the lateral transport at the heterointerface itself. Furthermore, we do not use the model to explain the length scale of the interfacial transport, instead reporting only our experimental observations.

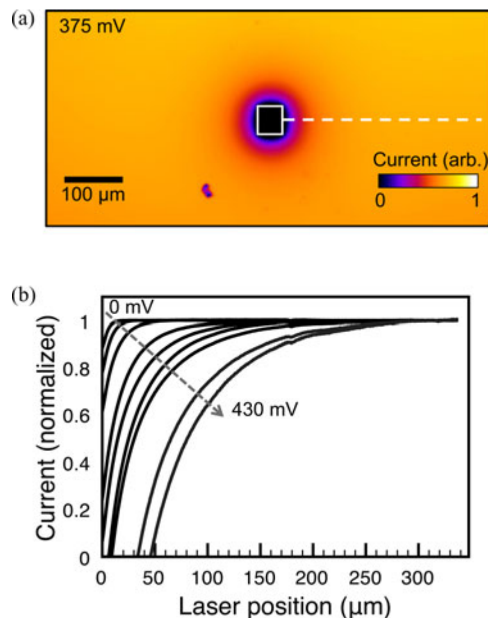

Fig. 3. LBIC measurements near a junction defect in an SHJ solar cell for a laser wavelength of 633 nm. The region indicated by the white box in (a) was irradiated with a dose of 6×10^{13} Ga ions/cm^2. (a) LBIC map around the defect when the cell is forward biased by 375 mV. (b) Normalized line profiles taken along the dashed white line shown in (a) for bias voltages of 0, 100, 200, 300, 350, 375, 400, 425, and 430 mV.

III. Results and Discussion

Fig. 3(a) shows an example of an LBIC image collected for the defect which was created with a dose of 6×10^{13} ions

cm^{-2}. The white box in Fig. 3(a) shows the location of the FIB-induced defect. Fig. 3(b) shows normalized profiles of the LBIC images taken along the dotted white line indicated in Fig. 3(a), with 0 corresponding to the edge of the ion-irradiated region. The profiles show that the lateral influence of the defective region increases as the forward bias is increased, thus increasing the effective cross-sectional area of the defect. The change in y-intercept for the profiles shown in Fig. 3(b) indicates that as the forward bias increases, the recombination activity of the defective region increases. This can be understood by noting that, as the device is forward biased, the electron concentration in the space-charge region increases by several orders of magnitude. This induces an increase in the recombination activity of any defect in that region according to Shockley–Read–Hall recombination statistics [30].

We attribute the increase in the effective cross section of the defect at forward bias to an increase in the average length along the a-Si:H/c-Si interface that a hole can traverse prior to collection out of the inversion layer. Carriers can participate in lateral conduction until they are either collected into the emitter and contribute to the measured photocurrent or are lost to other recombination processes along the pristine interface. We note that the increase of effective cross section observed here is not apparent in previous bias dependent LBIC measurements near grain boundaries in homojunction cells [31]. Recombination-active defects near the junction induce gradients in the quasi-Fermi levels and can even pin the Fermi level at mid gap. In the presence of high hole concentration in the inversion layer, even small gradients in the hole quasi-Fermi level can result in significant current flow because the hole current density $\overrightarrow{J_p}$ can be expressed as

$$\overrightarrow{J_p} = \mu_p p \nabla E_{Fp} \tag{1}$$

where μ_p is the hole mobility, p is the hold concentration, and E_{Fp} is the hole quasi-Fermi level [32].

The characteristic length over which carriers participate in lateral conduction induced by the defect is reflected in the shape of the LBIC profiles shown in Fig. 3(b). We quantified this characteristic distance over which holes are sensitive to the defect by fitting the normalized LBIC profiles to a simple empirical exponential function

$$1 - Ae^{-\frac{x}{L_h}} \tag{2}$$

which yields excellent fits to the data. Here, the parameter A is included to account for the fact that at changing bias, the y-intercept of the LBIC profile changes. Note that a negative y-intercept is possible at forward bias when there is not enough photocurrent to overcome the forward bias dark current of the device. The parameter of greatest interest, however, is L_h, which corresponds to the distance from the defect edge at which the photocurrent recovers to 1 – 1/e of its maximum value far from the defect relative to its value at the edge of the defective region. L_h is thus interpreted as the characteristic length scale over which holes in the inversion layer are sensitive to interface defects. Because hole transport in the inversion layer is a combination of drift and diffusion, L_h cannot be interpreted as a diffusion length.

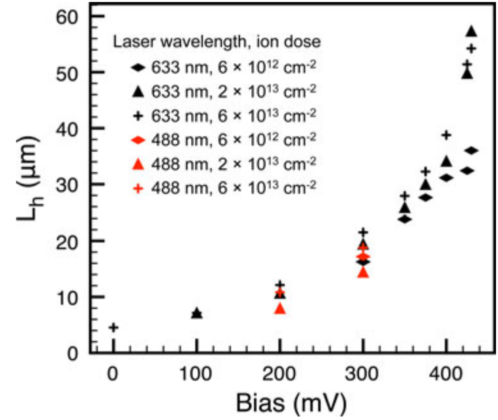

Fig. 4. Characteristic length scale (L_h) over which holes in the inversion layer are lost to recombination in a nearby junction defect. The values were extracted from line scans such as those shown in Fig. 3(b) for LBIC maps collected with laser excitation wavelengths of both 633 and 488 nm, varying applied forward bias, and different ion doses.

Fig. 4 shows how L_h changes with forward cell bias for three different defective-region ion doses. We note the general agreement between values of L_h for the three different ion doses, supporting our interpretation of L_h as a general parameter characterizing lateral hole transport length in pristine regions of the cell. We observe that L_h increases as forward bias is increased. We postulate that this increase in L_h is due to a reduced carrier collection rate of holes from the inversion layer because of a reduction in the strength of the junction electric field driving collection at forward bias. This would, in turn, increase the characteristic distance that holes would laterally traverse in the inversion layer prior to collection. While the processes governing carrier collection out of the inversion layer are not fully understood, time constants longer than 0.001 s have been reported for this process [21]. Using an estimate for the hole mobility in the near surface region of approximately 150 $cm^2 \cdot V^{-1} \cdot s^{-1}$ [18], a time constant of 0.001 s would yield an inversion layer diffusion length of 620 μm.

We observe values for L_h exceeding 50 μm. Note that, as discussed above, L_h in our results cannot be interpreted as a diffusion length. Using the area of a circle with a radius of 50 μm, we estimate that at defect densities of $\sim 10^4$ cm^{-2} and biases around 430 mV, the majority of carriers would be expected to encounter an interface defect. However, note that the ultimate impact of defects at any surface density on overall device performance will also be dependent on the capture cross section and associated recombination activity of the defect itself. Due to the experimental limitations discussed above, namely, that the laser-generated current must be larger than the forward bias dark current over the entire device area, we were not able to make measurements beyond 430 mV in forward bias, and L_h is expected to increase even further at higher biases. A typical SHJ cell operates at maximum power near 600 mV under 1-sun illumination; under these conditions, which also include long-wavelength illumination, carrier diffusion in the quasi-neutral

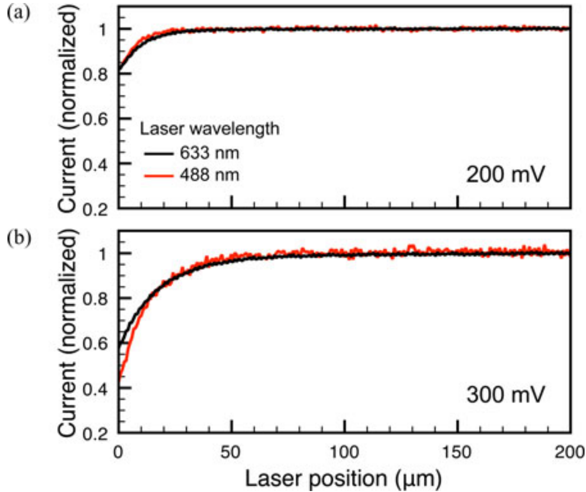

Fig. 5. LBIC profiles taken with laser wavelengths of 488 and 633 nm at forward biases of (a) 200 and (b) 300 mV. As in Fig. 3(b), the edge of the defect is located at a position of 0. The ion dose to the defective region was 2×10^{13} ions cm^2.

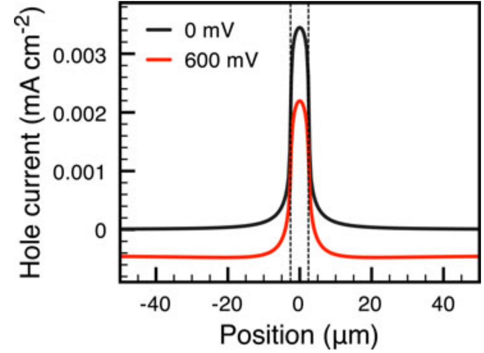

Fig. 6. Two-dimensional device simulation results showing that minimal lateral diffusion occurs prior to photogenerated carriers entering the inversion layer of a pristine SHJ cell via process (3) as pictured in Fig. 2, even at forward bias. The plot shows the y-component of the hole current density crossing the plane 40 nm below the heterojunction for cell biases of 0 and 600 mV. Illumination was with a 5-μm-wide beam of wavelength 633-nm light. The beam was centered at 0 on the x-axis, as indicated by the dashed lines. Positive current indicates flow toward the front of the device into the inversion layer.

bulk c-Si will also be an important transport mechanism affecting sensitivity to local defects.

An important point in the interpretation of our results is that the shape of the LBIC profile around the defect is representative of lateral transport in the inversion layer at the junction. Thus, it is important to rule out other routes carriers could take to recombine at the defect. One such pathway is transport through the TCO, which is much more conductive than the inversion layer [18]. As forward bias is increased, current may be injected from the TCO into the defect region, effectively functioning as a shunt. However, this is a source of dark current and occurs in forward bias independent of the local LBIC illumination. Therefore, contributions from this effect are manifested as a dc offset to the LBIC signal, as discussed in Section II, and do not affect the shape of the LBIC signal which we quantify with the parameter L_h in (2).

We also rule out diffusion in the quasi-neutral region of the base as an alternate pathway for carriers to reach the defect. This is supported by the agreement between the values of L_h measured with laser wavelengths of 488 and 633 nm, as shown in Fig. 4. The Beer–Lambert absorption lengths for c-Si at these wavelengths are 0.8 and 3 μm, respectively [33], and thus, the fraction of photocurrent generated in and near the depletion region changes for the two wavelengths; however, this does not correspond to a significant change in the measured lateral hole transport length, L_h. Thus, we conclude that the device physics governing L_h are dominated by carrier dynamics occurring *after* photogenerated holes enter the depletion region and are quickly swept into the inversion layer.

Fig. 5 further illustrates the agreement between the results obtained under varying laser wavelength. We note the change in y-intercept in Fig. 5(b), which we attribute to increased sampling of the defective near-surface region of the wafer at shorter wavelengths when the laser is directly illuminating the defective region. Because both excitation wavelengths have relatively shallow absorption depths, even as the depletion region shrinks in forward bias, carriers do not have to diffuse long distances to reach the front of the device and be collected. This kinetic argument regarding carrier transport in the c-Si is illustrated in the 2-D device simulation results shown in Fig. 6. The plot shows the y-component of the hole current crossing a horizontal plane 40 nm below the junction of an SHJ cell. Thus, it is a probe of the hole current profile undergoing process (3) in Fig. 2. The photocurrent in the simulation is generated by a 5-μm-wide beam of 633-nm light, and the simulation was carried out as described in Section II. A positive value indicates holes flowing toward the junction. It is apparent from the results that the shape of the carrier plume reaching the junction does not change significantly in forward bias. This is a result of the choice of a wavelength with a shallow absorption depth, preventing significant lateral diffusion in the quasi-neutral region prior to collection into the inversion layer. Also apparent in Fig. 6 is that at forward bias, the dark current injected across the junction away from the light beam increases, as indicated on the plot by a negative current.

IV. Conclusion

It is well established that interface defects in SHJ cells become increasingly detrimental to $V_{\rm oc}$ as the effective lifetime increases, since carriers can diffuse millimeters in the bulk of a high-lifetime cell under open-circuit conditions. Our experiments show that, in SHJ cells, localized surface defects also reduce carrier collection at voltages below typical maximum-power-point and open-circuit biases. Our interpretation of the results is that this is a consequence of the inversion layer created by the valence band offset at the a-Si:H/c-Si interface; while holes dwell in the inversion layer prior to collection, they may diffuse or drift laterally for tens of microns, increasing the probability that they will encounter a defect and recombine. Thus, according to the lateral inversion layer transport mechanism proposed here, transport in the inversion layer contributes to the sensitivity that SHJ cells are known to show to interface quality. We observe that the length scale over which carriers are sensitive to defects increases in forward bias. The bias dependence of our results below the maximum power point suggests that high-quality interfaces are important not just for high $V_{\rm oc}$,

but for optimum fill factor as well, and demonstrates that controlling surface quality is important for full optimization of the current–voltage behavior of SHJ cells.

ACKNOWLEDGMENT

The authors gratefully acknowledge insightful conversations with D. Young and S. Grover from the National Renewable Energy Laboratory and with M. Filipič from the University of Ljubljana. They also gratefully acknowledge critical support and infrastructure provided for this work by the Kavli Nanoscience Institute at Caltech.

REFERENCES

[1] W. G. van Sark, L. Korte, and F. Roca, *Physics and Technology of Amorphous–Crystalline Heterostructure Silicon Solar Cells*. New York, NY, USA: Springer, 2012.

[2] S. De Wolf, A. Descoeudres, Z. C. Holman, and C. Ballif, "High-efficiency silicon heterojunction solar cells: A review," *Green*, vol. 2, no. 1, pp. 7–24, 2012.

[3] M. Tanaka, M. Taguchi, T. Matsuyama, T. Sawada, S. Tsuda, S. Nakano, H. Hanafusa, and Y. Kuwano, "Development of new a-Si/c-Si heterojunction solar cells: ACJ-HIT (artificially constructed junction-heterojunction with intrinsic thin-layer)," *Jpn. J. Appl. Phys.*, vol. 31, pp. 3518–3522, 1992.

[4] T. Mishima, M. Taguchi, H. Sakata, and E. Maruyama, "Development status of high-efficiency HIT solar cells," *Solar Energy Mater. Solar Cells*, vol. 95, no. 1, pp. 18–21, 2011.

[5] M. Taguchi, A. Terakawa, E. Maruyama, and M. Tanaka, "Obtaining a higher V_{oc} in HIT cells," *Progr. Photovoltaics, Res. Appl.*, vol. 13, no. 6, pp. 481–488, 2005.

[6] M. Taguchi, E. Maruyama, and M. Tanaka, "Temperature dependence of amorphous/crystalline silicon heterojunction solar cells," *Jpn. J. Appl. Phys.*, vol. 47, no. 2, pp. 814–818, 2008.

[7] D. M. Powell, M. T. Winkler, H. J. Choi, C. B. Simmons, D. B. Needleman, and T. Buonassisi, "Crystalline silicon photovoltaics: A cost analysis framework for determining technology pathways to reach baseload electricity costs," *Energy Environ. Sci.*, vol. 5, pp. 5874–5883, 2012.

[8] T. Wang, E. Iwaniczko, M. Page, D. Levi, Y. Yan, H. Branz, and Q. Wang, "Effect of emitter deposition temperature on surface passivation in hot-wire chemical vapor deposited silicon heterojunction solar cells," *Thin Solid Films*, vol. 501, no. 1–2, pp. 284–287, 2006.

[9] H. Fujiwara and M. Kondo, "Impact of epitaxial growth at the heterointerface of a-Si:H/c-Si solar cells," *Appl. Phys. Lett.*, vol. 90, pp. 013503-1–013503-3, 2007.

[10] S. De Wolf and M. Kondo, "Abruptness of a-Si:H/c-Si interface revealed by carrier lifetime measurements," *Appl. Phys. Lett.*, vol. 90, pp. 042111-1–042111-3, 2007.

[11] K.-S. Ji, J. Choi, H. Yang, H.-M. Lee, and D. Kim, "A study of crystallinity in amorphous Si thin films for silicon heterojunction solar cells," *Solar Energy Mater. Solar Cells*, vol. 95, no. 1, pp. 203–206, 2011.

[12] J. Geissbuhler, S. De Wolf, B. Demaurex, J. P. Seif, D. T. L. Alexander, L. Barraud, and C. Ballif, "Amorphous/crystalline silicon interface defects induced by hydrogen plasma treatments," *Appl. Phys. Lett.*, vol. 102, pp. 231604-1–231604-5, 2013.

[13] J. P. Kleider, J. Alvarez, A. V. Ankudinov, A. S. Gudovskikh, E. V. Gushina, M. Labrune, O. A. Maslova, W. Favre, M. E. Gueunier-Farret, P. R. i Cabarrocas, and E. I. Terukov, "Characterization of silicon heterojunctions for solar cells," *Nanoscale Res. Lett.*, vol. 6, p. 152, 2011.

[14] J. V. Li, R. S. Crandall, D. L. Young, M. R. Page, E. Iwaniczko, and Q. Wang, "Capacitance study of inversion at the amorphous-crystalline interface of n-type silicon heterojunction solar cells," *J. Appl. Phys.*, vol. 110, no. 11, p. 114502, 2011.

[15] J. P. Kleider, Y. Soro, R. Chouffot, A. Gudovskikh, P. R. i Cabarrocas, J. Damon- Lacoste, D. Eon, and P.-J. Ribeyron, "High interfacial conductivity at amorphous silicon/crystalline silicon heterojunctions," *J. Non-Crystalline Solids*, vol. 354, pp. 2641–2645, 2008.

[16] W. Favre, M. Labrune, F. Dadouche, A. S. Gudovskikh, P. R. i. Cabarrocas, and J. P. Kleider, "Study of the interfacial properties of amorphous silicon/n-type crystalline silicon heterojunction through static planar conductance measurements," *Phys. Status Solidi (c)*, vol. 7, no. 3/4, pp. 1037–1040, 2010.

[17] K. Ghosh, C. Tracy, and S. Bowden, "Experimental and theoretical verification of the presence of inversion region in a-Si/c-Si heterojunction solar cells with an intrinsic layer," in *Proc. 38th IEEE Photovoltaic Spec. Conf.*, 2012, pp. 001046–001048.

[18] M. Filipič, Z. C. Holman, F. Smole, S. De Wolf, C. Ballif, and M. Topic, "Analysis of lateral transport through the inversion layer in amorphous silicon/crystalline silicon heterojunction solar cells," *J. Appl. Phys.*, vol. 114, p. 074504, 2013.

[19] A. Kanevce and W. K. Metzger, "The role of amorphous silicon and tunneling in heterojunction with intrinsic thin layer (HIT) solar cells," *J. Appl. Phys.*, vol. 105, no. 9, p. 094507, 2009.

[20] K. Ghosh, S. Bowden, and C. Tracy, "Role of hot carriers in the interfacial transport in amorphous silicon/crystalline silicon heterostructure solar cells," *Phys. Status Solidi (a)*, vol. 210, pp. 413–419, 2013.

[21] R. S. Crandall, E. Iwaniczko, J. V. Li, and M. R. Page, "A comprehensive study of hole collection in heterojunction solar cells," *J. Appl. Phys.*, vol. 112, no. 9, p. 093713, 2012.

[22] M. G. Deceglie and H. A. Atwater, "Effect of defect-rich epitaxy on crystalline silicon/amorphous silicon heterojunction solar cells and the use of low-mobility layers to improve performance," in *Proc. 37th IEEE Photovoltaic Spec. Conf.*, 2011, pp. 001417–001429.

[23] Z. C. Holman, A. Descoeudres, L. Barraud, F. Z. Fernandez, J.P. Seif, S. De Wolf, and C. Ballif, "Current losses at the front of silicon heterojunction solar cells," *IEEE J. Photovoltaics*, vol. 2, no. 1, pp. 7–15, Jan. 2012.

[24] A. Descoeudres, L. Barraud, S. De Wolf, B. Strahm, D. Lachenal, C. Guerin, Z. C. Holman, F. Zicarelli, B. Demaurex, J. Seif, J. Holovsky, and C. Ballif, "Improved amorphous/crystalline silicon interface passivation by hydrogen plasma treatment," *Appl. Phys. Lett.*, vol. 99, no. 12, p. 123506, 2011.

[25] A. Descoeudres, Z. Holman, L. Barraud, S. Morel, S. De Wolf, and C. Ballif, "$>$21% efficient silicon heterojunction solar cells on n- and p-type wafers compared," *IEEE J. Photovoltaics*, vol. 3, no. 1, pp. 83–89, Jan. 2013.

[26] Z. C. Holman, M. Filipic, A. Descoeudres, S. De Wolf, F. Smole, M. Topic, and C. Ballif, "Infrared light management in high-efficiency silicon heterojunction and rear-passivated solar cells," *J. Appl. Phys.*, vol. 113, no. 1, p. 013107, 2013.

[27] J. Ziegler and J. Biersack, SRIM-2008, Stopping power and range of ions in matter, 2008.

[28] TCAD Sentaurus. [Online]. Available: http://www.synopsys.com

[29] R. E. I. Schropp and M. Zeman, *Amorphous and Microcrystalline Silicon Solar Cells: Modeling, Materials and Device Technology*. Norwell, MA, USA: Kluwer, 1998.

[30] S. Grover, C. W. Teplin, J. V. Li, D. C. Bobela, J. Bornstein, P. Schroeter, S. Johnston, H. Guthrey, P. Stradins, H. M. Branz, and D. L. Young, "Device physics of heteroepitaxial film c-si heterojunction solar cells," *IEEE J. Photovoltaics*, vol. 3, no. 1, pp. 230–235, Jan. 2013.

[31] F. J. Vorster and E. E. van Dyk, "Bias-dependent high saturation solar LBIC scanning of solar cells," *Solar Energy Mater. Solar Cells*, vol. 91, no. 10, pp. 871–876, 2007.

[32] S. Sze and K. Ng., *Physics of Semiconductor Devices*. New York, NY, USA: Wiley-Interscience, 2007.

[33] M. A. Green and M. J. Keevers, "Optical properties of intrinsic silicon at 300 K," *Progr. Photovoltaics, Res. Appl.*, vol. 3, no. 3, pp. 189–192, 1995.

Authors' photographs and biographies not available at the time of publication.